



Deposited via The University of Sheffield.

White Rose Research Online URL for this paper:

<https://eprints.whiterose.ac.uk/id/eprint/211713/>

Version: Published Version

---

**Article:**

Carter, L.J., Dennis, S., Allen, K. et al. (2023) Mitigating contaminant-driven risks for the safe expansion of the agricultural–sanitation circular economy in an urbanizing world. *ACS ES&T Water*, 4 (4). pp. 1166-1176. ISSN: 2690-0637

<https://doi.org/10.1021/acsestwater.3c00803>

---

**Reuse**

This article is distributed under the terms of the Creative Commons Attribution (CC BY) licence. This licence allows you to distribute, remix, tweak, and build upon the work, even commercially, as long as you credit the authors for the original work. More information and the full terms of the licence here:

<https://creativecommons.org/licenses/>

**Takedown**

If you consider content in White Rose Research Online to be in breach of UK law, please notify us by emailing [eprints@whiterose.ac.uk](mailto:eprints@whiterose.ac.uk) including the URL of the record and the reason for the withdrawal request.

# Synthesis of Fluorinated Amphiphilic Polymers and the Morphological Dependence on Their Oxygen Binding Capacity

Zerui Chen and Lance J. Twyman\*

Cite This: *ACS Appl. Polym. Mater.* 2024, 6, 4164–4170

Read Online

ACCESS |



Metrics &amp; More

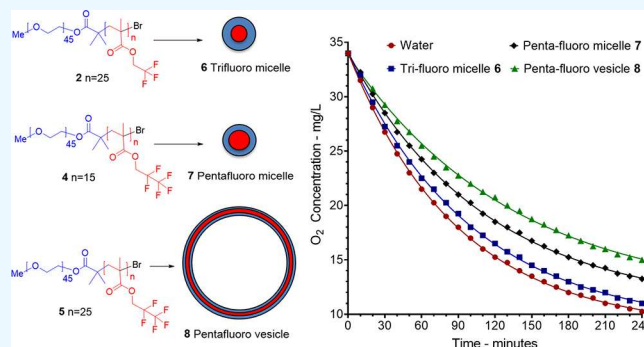


Article Recommendations



Supporting Information

**ABSTRACT:** Water-soluble materials that can bind, sense, and deliver oxygen are important for several applications. These include catalysis, environmental sensors, smart packaging, agriculture, and medicine. Herein we report the synthesis of two related fluorinated amphiphilic polymers that can self-assemble into small micelles (20–30 nm) or larger vesicles (>300 nm). We found that the oxygen binding capacity of these polymers was dependent on the morphology of their self-assembled structures. At a constant fluorine concentration of 1.5 mg/mL, the oxygen solubility within the vesicle solution was 55% higher than that measured in pure water and 25% higher than the corresponding micelle solution. The increased concentration of oxygen in the vesicle solution indicated a significantly higher level of oxygen binding, which was attributed to additional oxygen trapped within



the vesicle's aqueous interior.

**KEYWORDS:** diblock polymer, fluorinated polymer, oxygen carrier, self-assembly, biocompatibility, vesicle

## 1. INTRODUCTION

Oxygen is a versatile element that has many applications in various fields of science and technology. These include materials that can catalyze oxidation reactions,<sup>1–3</sup> monitor oxygen levels in food and packaging,<sup>4</sup> in oxygen sensing,<sup>5,6</sup> assessing and improving the quality/purity of water in the environment,<sup>7</sup> and in agriculture.<sup>8</sup> In addition, oxygen-containing nanomaterials have shown promise in a number of medical applications, including photodynamic therapy and MRI imaging.<sup>9,10</sup> The work described in this paper is concerned with the use of synthetic oxygen carriers for use as an artificial blood product.<sup>11</sup> In medical emergencies, rapid replacement and restoration of blood volume are crucial to prevent death due to loss of blood volume. Traditionally, this is achieved using transfusion of donated blood, but this is expensive and has problems with contamination and storage. Furthermore, transfusion of donated blood is not practical or ideal in a challenging trauma situation, i.e., the scene of an accident, a natural disaster, or the battlefield. In these situations, death can occur through a simple loss of blood volume, and a simple plasma solution (an aqueous solution of coagulant, proteins, electrolytes, and sugars) is used to replace the lost blood volume. However, a better solution would be to administer an alternative plasma solution that could function as a volume expander to replace the lost volume of blood but could also bind, deliver, and release oxygen. There have been many attempts to address this challenge, including the use of synthetically modified hemoglobin-based carriers<sup>12</sup> and bio-

mimetic iron(II)porphyrin-based structures.<sup>13</sup> Unfortunately, none of these systems had any clinical success.

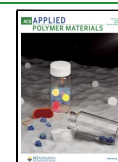
In a completely different approach, small fluorine-containing molecules known as perfluorocarbons (PFCs) can dissolve large amounts of oxygen in aqueous solution.<sup>14,15</sup> However, these molecules have a very low solubility in water and must be administered as a stabilized emulsion. Although there was some early promise for PFCs as blood substitutes, they have not been widely adopted due to their high cost and potential side effects. These include extremely long half-life, fluorine accumulation in tissue, poor excretion, fever and flu-like symptoms, and, in extreme cases, death.<sup>16,17</sup> To address these issues, we recently developed and reported the synthesis of a series of fluorinated diblock polymer micelles and showed how these could accommodate relatively large amounts of oxygen within their fluorinated interior, leading to a large increase in the concentration of oxygen in water. The level of oxygen binding was dependent on the size of the polymer and the concentration.<sup>18</sup> Although this strategy has the potential to eliminate the problems associated with the use of small fluorine-containing molecules, the size of the polymeric

Received: January 24, 2024

Revised: March 27, 2024

Accepted: March 27, 2024

Published: April 2, 2024



micelles was smaller than the pore size in some vessel walls (100 nm).<sup>19</sup> This would result in leakage from the vascular system and accumulation in the tissue (leading to toxic side effects). To overcome these size-related problems and to create a system that could dissolve more oxygen, we proposed the use of an alternative diblock polymer that could self-assemble into a vesicle.<sup>20</sup> Polymer vesicles are much larger than the pore size of most vessel walls and therefore less likely to leak out of the vascular system. As such, the circulation times and oxygen levels were significantly improved. In addition to synthesizing a larger aggregate, we also proposed the use a monomer that contained more fluorine than previously used.<sup>18</sup> This should generate a more fluorine dense region in the core of the micelle or vesicle membrane, leading to an increase in the measured solubility of oxygen. This hypothesis would be tested and compared to a polymeric micelle synthesized from a monomer with fewer fluorines.

## 2. EXPERIMENTAL SECTION

**2.1. Materials.** 2,2,3,3,3-Pentafluoropropyl methacrylate and 2,2,2-trifluoroethyl methacrylate (purchased from Fluochem) were purified by passing them through a basic aluminum oxide column and then storing them in the fridge at 4 °C. Toluene (HPLC grade), ethanol (HPLC grade), and dichloromethane (DCM, HPLC grade) were purchased from Fisher Chemical and used as supplied. Triethylamine (distilled prior to use), basic aluminum oxide, and diethyl ether were purchased from Prolabo. Methyl poly(ethylene glycol) 2000,  $\alpha$ -bromoisobutyl bromide, and *N,N,N',N',N'*-pentamethyldiethylenetriamine (PMDETA) were purchased from Sigma-Aldrich and used as supplied. Copper(I) bromide was purchased from Sigma-Aldrich and was cleaned prior to use by washing with glacial acetic acid, ethanol, and diethyl ether (repeated until the supernatant was colorless). The clean copper bromide was then dried in a vacuum oven at 40 °C overnight and stored in a dark, dry environment.

**2.2. Instrumentation.** <sup>1</sup>H NMR, <sup>13</sup>C NMR, and <sup>19</sup>F NMR spectra were obtained using a Bruker Avance DPX 400 instrument. The chemical shift was calibrated by reference to residual solvent signals and reported as ppm. The data were analyzed the MestReNova software. FT-IR spectra was obtained using a PerkinElmer UATR Two instrument. Spectra were obtained at 4 cm<sup>-1</sup> resolution, averaging 16 scans. DLS analysis was performed by a Malvern Zetasizer nano, and the measurement angle was set as 173° backscatter. Samples were tested at 25 °C and measured 50 times to get a number-average size result. Measurements were performed at a concentration slightly higher than that used to record oxygen binding (2.5 mg/mL).

**2.3. Synthesis. Methyl Poly(Ethylene glycol) Bromide (MPEG-Br).** A solution of mPEG in toluene (20 g, 0.01 mol, 100 mL) was azeotropically dried by evaporating the solvent by rotary evaporation. The solid was redissolved in 250 mL of toluene and cooled to 0 °C. Triethylamine (1.45 g, 0.0143 mol) was added to the solution.  $\alpha$ -Bromoisobutyl bromide (2.79 g, 0.0121 mol) was added, and the solution was stirred for 1 h. The solution was then allowed to warm to room temperature, and stirring continued for a further 24 h. The solution was filtered and then dropped into diethyl ether to obtain the crude product. The crude product was recrystallized in ethanol to obtain pure product, which was collected by filtration and then dried in a vacuum oven at 40 °C to obtain mPEG-Br as a white solid. <sup>1</sup>H NMR (400 MHz, CDCl<sub>3</sub>,  $\delta$ ): 1.95 (s, -COOBr(CH<sub>3</sub>)<sub>2</sub>), 3.4 (s, CH<sub>3</sub>O-), 3.66 (s, -OCH<sub>2</sub>CH<sub>2</sub>O-), 4.34 (t, -CH<sub>2</sub>OOCMe<sub>2</sub>bBr). FTIR (cm<sup>-1</sup>): 2885 (C-H stretch), 1110 (C-O stretch). GPC (LMW; THF):  $M_n = 2874$  g/mol,  $M_w/M_n = 1.041$ . Yield: 14 g, 70%.

**General Synthesis of MPEG-Poly(pentafluoropropyl methacrylate)<sub>n</sub> Block Polymers (mPEG-PPF<sub>n</sub>).** mPEG-Br (2.15 g, 0.001 mol) was dissolved in 10 mL of toluene and placed into a Schlenk tube. The solution was then degassed three times under freeze-thaw conditions. Copper bromide (0.144 g, 0.001 mol) was then added in

one portion, followed by pentafluoro methacrylate, which was added by syringe. The mixture was then degassed a further three times under freeze thaw conditions, before PMDETA (0.249 g, 0.003 mol) was added by syringe. The reaction mixture was then stirred under nitrogen at 70 °C overnight. After that, the reaction was allowed to warm to room temperature before an excess of toluene was added. The solution was filtered and concentrated in a rotary evaporator. The resulting solid was purified using a basic alumina column and dichloromethane as an eluent. The eluent solution was then concentrated by rotary evaporation. The pure product was precipitated from petroleum ether and then dried in a vacuum oven at 40 °C.

**mPEG-PPF<sub>15</sub> 4.** The general method described above was used in the following amounts. mPEG-Br (2.15 g, 1 mmol) was reacted with 2,2,3,3,3-pentafluoropropyl methacrylate (2.56 mL, 15 mmol) to obtain mPEG-PPF<sub>15</sub> 4 as a solid. <sup>1</sup>H NMR (400 MHz; CDCl<sub>3</sub>; ppm): 0.80–1.20 (d, -CH<sub>2</sub>C(CH<sub>3</sub>)CO; s, -COC(CH<sub>3</sub>)<sub>2</sub>), 1.85–2.21 (d, -CH<sub>2</sub>C(CH<sub>3</sub>)CO), 3.40 (s, CH<sub>3</sub>O-),  $\delta$  3.67 (s, -OCH<sub>2</sub>CH<sub>2</sub>O-), 4.36 (t, -CH<sub>2</sub>CF<sub>2</sub>CF<sub>3</sub>). <sup>19</sup>F NMR (100 MHz; CDCl<sub>3</sub>; ppm): -83.5 (s, -CF<sub>3</sub>), -123 (s, -CH<sub>2</sub>CF<sub>2</sub>-). FTIR (cm<sup>-1</sup>): 2885 (s, C-H stretch), 1738 (s, C=O stretch), 1194 and 1140 (s, C-F stretch), 1110 (s, C-O stretch). GPC (LMW; THF):  $M_n = 4742$  g/mol,  $M_w/M_n = 1.28$ .

**mPEG-PPF<sub>25</sub> 5.** The general method described above was used with the following specific amounts. mPEG-Br (2.15 g, 1 mmol) and 2,2,3,3,3-pentafluoropropyl methacrylate (4.26 mL, 25 mmol) to obtain mPEG-PPF<sub>25</sub> 5 as a solid. <sup>1</sup>H NMR (400 MHz; CDCl<sub>3</sub>; ppm): 0.80–1.20 (d, -CH<sub>2</sub>C(CH<sub>3</sub>)CO; s, -COC(CH<sub>3</sub>)<sub>2</sub>), 1.85–2.21 (d, -CH<sub>2</sub>C(CH<sub>3</sub>)CO), 3.40 (s, CH<sub>3</sub>O-), 3.67 (s, -OCH<sub>2</sub>CH<sub>2</sub>O-), 4.36 (t, -CH<sub>2</sub>CF<sub>2</sub>CF<sub>3</sub>). <sup>19</sup>F NMR (100 MHz; CDCl<sub>3</sub>; ppm): -83.5 (s, -CF<sub>3</sub>), -123 (s, -CH<sub>2</sub>CF<sub>2</sub>-). FTIR (cm<sup>-1</sup>): 2885 (s, C-H stretch), 1738 (s, C=O stretch), 1194 and ~1140 (s, C-F stretch), 1110 (s, C-O stretch). GPC (LMW; THF):  $M_n = 4939$  g/mol,  $M_w/M_n = 1.19$ .

**mPEG-PMMA<sub>21</sub> 9.** The general method described above for the fluorinated polymers was used with the following specific amounts. mPEG-Br (2.15 g, 1 mmol) was reacted with methyl methacrylate (2.1 mL, 20 mmol) and PMDETA (0.251 mL, 1.2 mmol) to give mPEG-*b*-PMMA<sub>21</sub> as a solid (3.14 g, 77%). <sup>1</sup>H NMR (400 MHz; CDCl<sub>3</sub>; ppm):  $\delta$  0.80–1.09 (m, 63H, -CO(CH<sub>3</sub>)), 1.09–2.0 (m, 43H, -CH<sub>2</sub>-CO(CH<sub>3</sub>)), 3.40 (s, 3H, CH<sub>3</sub>O-), 3.66 (s, 180H, -OCH<sub>2</sub>CH<sub>2</sub>O-), 3.62 (s, 64H, -COOCH<sub>3</sub>). GPC (LMW; THF):  $M_n = 5100$ ,  $M_w/M_n = 1.15$

**Determination of Critical Aggregation Concentration (CAC).**<sup>21</sup> A polymer solution was prepared by dissolving 20 mg of the polymer in 2 mL of THF and 20 mL of deionized water. The THF was then evaporated, and 0.5 mL of a pyrene in acetone solution (0.01 mg/mL) was added. The solution was then topped back up to 20 mL with deionized water to give a 1 mg/mL polymer-micelle stock solution, which was used to make solutions with concentrations ranging from 0.4 to 0.0006 mg/mL. The CAC measurements were conducted on a FluoroMax-4 spectrometer with an excitation wavelength of 334 nm, and the emission spectrum recorded from 350 to 450 nm; the excitation/emission slits were set as 2.5/2.5 mm. The CAC for each polymer was measured three times to obtain an average value.

**Measurement of Dissolved Oxygen.**<sup>18</sup> Measurements were obtained using a Mettler Toledo S9 Seven2Go Pro with Inlab@ Optiox probe, which was calibrated at saturated vapor 1 day prior to use. Samples were dispersed in 20 mL of deionized water and stirred at 300 rpm at 30 °C until the temperature was stable. Pure oxygen was bubbled through the samples until the concentration stopped increasing and reached a maximum level (34 mg/L). At this point, oxygen bubbling was stopped, and real-time oxygen concentrations were collected every 10 s for 240 s.

## 3. RESULTS AND DISCUSSION

In previous work, we had used 2,2,2-trifluoroethyl methacrylate (1) as the monomer to synthesize the diblock mPEG-poly(2,2,2-trifluoroethyl methacrylate) (2). Diblock polymer

## Scheme 1. Synthesis of the Tri- and Penta-Polyfluoro Diblock Polymers

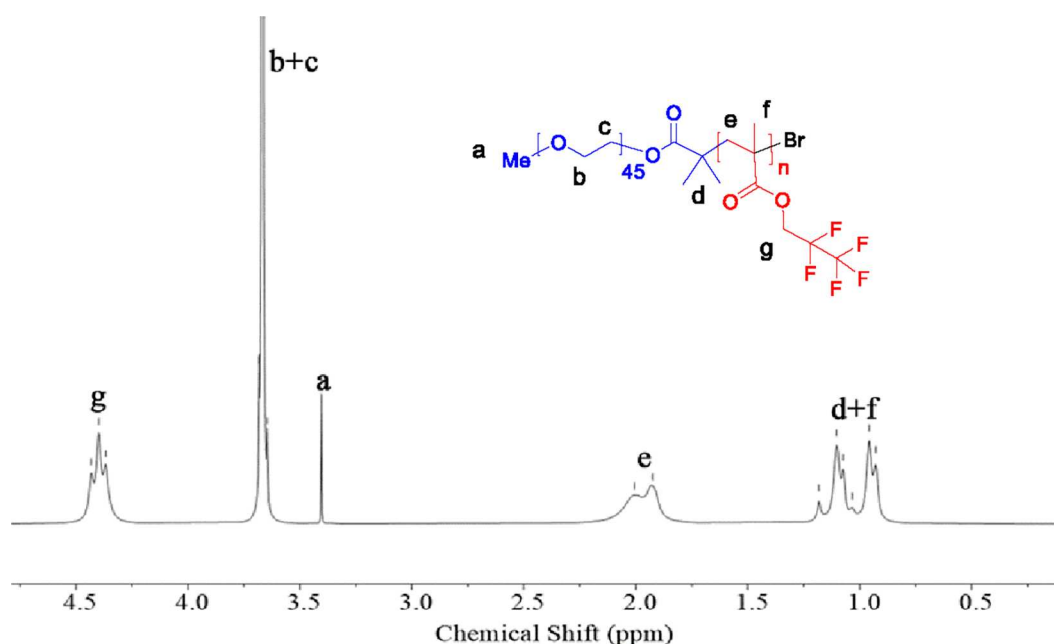
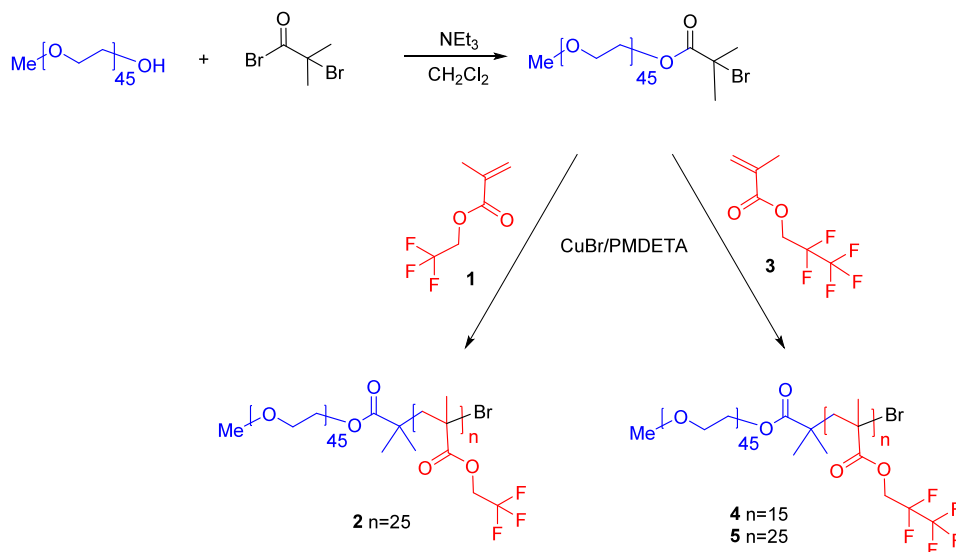


**Figure 1.**  $^1\text{H}$  NMR spectra of the diblock polymer mPEG-PPF<sub>15</sub>. Labels a–g on the structure correspond to signal peaks labeled a–g on spectra.

2, with a degree of polymerization equal to 25, would be used as a control polymer and is termed mPEG-PTF<sub>25</sub> 2 for simplicity.<sup>18</sup> But for the work described herein, 2,2,3,3,3-pentafluoropropyl methacrylate (3) was used. This is larger than the trifluoro monomer, so it will occupy more space in the self-assembled structures. Therefore, degrees of polymerization equal to 15 and 25 were targeted for the micelle and vesicle, respectively.<sup>22</sup> The pentafluoro monomer 3 was polymerized using the macroinitiator poly(ethylene glycol)methyl ether-2-bromoisobutyrate, and an atom transfer radical polymerization (ATRP),<sup>23</sup> to give the fluorine-rich diblock polymers mPEG-poly(2,2,3,3,3-pentafluoroethyl methacrylate) 4 and 5 (mPEG-PPF<sub>15</sub> and mPEG-PPF<sub>25</sub>). The synthesis and characterization details of a control polymer 2, prepared using 2,2,2-trifluoroethyl methacrylate, which has three fluorines per monomer, has been reported previously.<sup>18</sup> The syntheses of all compounds are shown in Scheme 1.  $^1\text{H}$  NMR confirmed the

structure of polymers 4 and 5, with a large singlet for the  $\text{CH}_2$ -mPEG backbone visible at 3.66 ppm in the  $^1\text{H}$  NMR spectrum and a smaller singlet at 3.40 ppm for the terminal OMe group. There was also a triplet at a relatively high field (4.39 ppm) with a relatively large coupling constant (12 Hz), corresponding to the hydrogens adjacent to the  $\text{C}_2\text{F}_5$  group. Additionally, peaks were observed between 1.46 and 2.24 ppm for the protons on the fluoro block's backbone (Figures S1 and S2 in the Supporting Information). Signals at  $-84$  and  $-123$  ppm in  $^{19}\text{F}$  NMR were attributed to the  $\text{CF}_3$ - and  $-\text{CF}_2$ -, respectively (Figure S3). Diblock polymers, which consist of two segments that have significant differences in refraction index, can produce bimodal negative peaks in their GPC traces.<sup>18,24,25</sup> This is a known phenomenon and present in our systems, making it challenging to accurately determine  $M_n$  and  $M_w$ . Nevertheless, molecular weights ( $M_n$ ) could be determined using  $^1\text{H}$  NMR by analyzing the integration ratios

of the terminal  $\text{CH}_3$  peak from the mPEG block and the  $-\text{CH}_2-$  resonance of the protons nearest the fluoro group (labeled “a” and “g”, respectively in Figure 1). The  $M_n$  data for each polymer were then used to obtain the degrees of polymerization for each polymer, which were similar to those targeted. The molecular weights and DP data for all of the polymers are shown in Table 1. Although GPC could not be

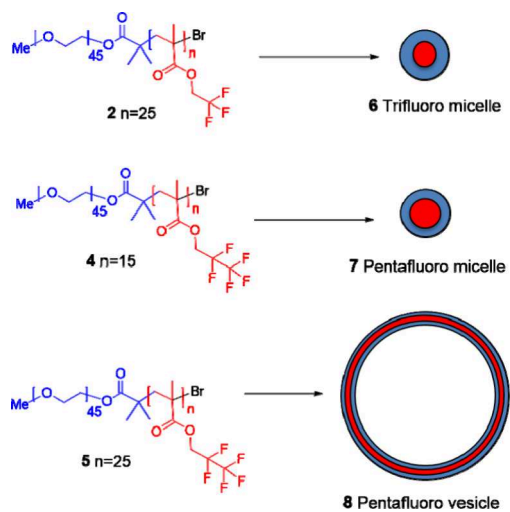
**Table 1. Molecular Weight and CAC Data for the Tri- and Penta-Polyfluoro Diblock Polymers**

diblock	target DP	actual DP	$M_n$ ( $^1\text{H}$ NMR) (Da)	CAC ( $\mu\text{g}/\text{mL}$ )
mPEG-PTF <sub>25</sub> 2	25	25	6200	3.5
mPEG-PPF <sub>15</sub> 4	15	17	5924	5.0
mPEG-PPF <sub>25</sub> 5	25	25	7450	5.0

used to estimate  $M_n/M_w$  with any degree of accuracy, the absence of a peak for the PEG macroinitiator did confirm that the diblock polymers were not contaminated or mixed with the PEG macroinitiator.

Aggregation of the polymers into various nanostructures is shown in Scheme 2. The aggregation was initially evaluated by

**Scheme 2. Aqueous Self-Assembly of the Tri- and Penta-Polyfluoro Diblock Polymers into Micelles and Vesicles**



the measurement of the critical aggregation concentrations (CAC). These were determined using the pyrene method, which plots changes in the intensity ratio of the pyrene fluorescent peaks at 373 and 383 nm, with respect to polymer concentration.<sup>21,26</sup> For the pentafluoro polymers (mPEG-PPF<sub>15/25</sub>) 4 and 5, a CAC of 5  $\mu\text{g}/\text{mL}$  was measured. This compares to a CAC of 3.5  $\mu\text{g}/\text{mL}$  for trifluoro polymer 2 (mPEG-PTF<sub>25</sub>). Dynamic light scattering (DLS) was used to verify aggregation and determine the size and morphology of the aggregated nanostructures. Solutions were made by dissolving the polymers in 2 mL of THF, followed by slow addition of deionized water (20 mL) with vigorous stirring.<sup>27</sup> The solutions were then concentrated using a rotary evaporator to remove the THF, and the volume was topped up to 20 mL with deionized water. DLS measurements were then measured above and below the CMC. For the trifluoro mPEG-PTF<sub>25</sub> polymer, particles with an average diameter around 22 nm were observed.<sup>18</sup> A slightly larger diameter of 30

nm was recorded for the pentafluoro mPEG-PPF<sub>15</sub> polymer 4 (Figure 2, top). However, when the pentafluoro polymer

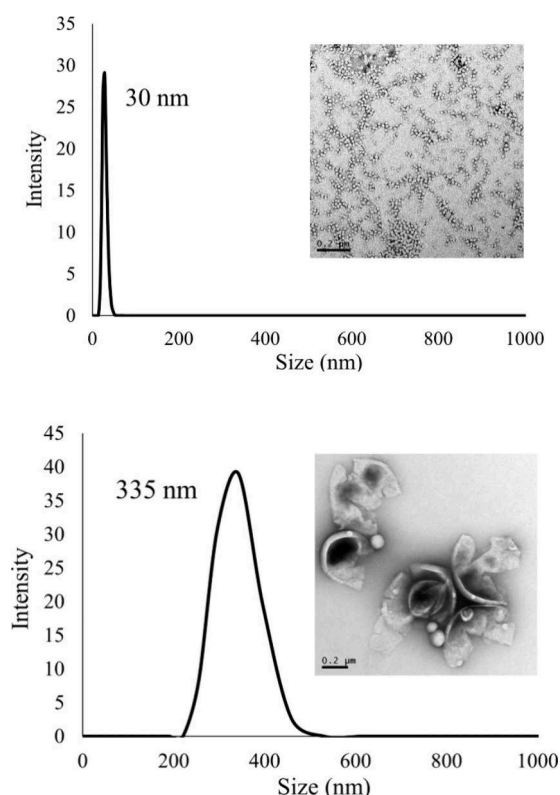


**Figure 2.** DLS images of the pentafluoropolymer 4 (top) and the pentafluoropolymer 5 (bottom). Insets show the TEM images of the aggregated structures; scale bar is 0.2  $\mu\text{m}$  (micelle 7 and fractured vesicle 8). DLS and TEM experiments were performed at the same concentration used for the oxygen binding experiments described below.

mPEG-PPF<sub>25</sub> 5 was assessed, a structure with an average diameter of 335 nm was observed (Figure 2, bottom). No peaks in the DLS could be detected for any of the polymers when measured at concentrations below their CMC. The DLS data were confirmed by TEM images, which showed an even distribution of small spherical particles with diameters around 30 nm for the trifluoro mPEG-PTF<sub>25</sub> polymer 2<sup>18</sup> and the pentafluoro mPEG-PPF<sub>15</sub> polymer 4. This confirms the micellar structure of these polymers. When viewing the TEM images of the pentafluoro polymer mPEG-PPF<sub>25</sub> 5, larger structures with sizes around 200–400 nm were observed. However, the images showed broken or fractured vesicles, presumably due to their instability in the nonaqueous environment of TEM. The phenomenon has been reported previously for amphiphilic block copolymer vesicles.<sup>28,29</sup> Nonetheless, the shapes and the sizes observed are consistent with vesicle structures in aqueous solution.<sup>30</sup>

The oxygen carrying properties of the new materials were tested using various solutions of the polymers at constant fluorine concentration. The experiments involved saturating solutions with 100% pure oxygen and measuring the time taken for the oxygen concentrations to equilibrate with air, where the level of oxygen is just 21%. Oxygen levels in the solution were measured by using a dissolved oxygen probe. However, this can only detect the oxygen in bulk solution and cannot directly measure or detect any oxygen encapsulated

within the self-assembled structures. Nevertheless, as the saturated solutions equilibrate with the oxygen levels in air, there is “space” in the solution that encapsulated oxygen can fill. This has the effect of lengthening the time for the oxygen levels in solution to reach equilibrium. These times/half-lives can be measured, and any differences in rate will be related to oxygen encapsulation within the various self-assembled structures. The process for a micelle is shown schematically in Figure 3. This is an established method and has previously been used to measure oxygen content and release from perfluoro carbon systems<sup>32</sup> and fluoro polymers.<sup>18,33,34</sup>

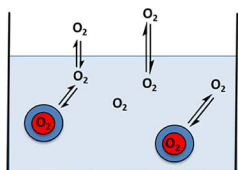


**Figure 3.** Schematic showing oxygen binding and release equilibria from a micellar solution saturated with 100% oxygen. The oxygen bound in the micelle can leave only after oxygen from the saturated solution equilibrates with the levels of oxygen in air.

Oxygen levels were measured using a Mettler Toledo Seven2Go dissolved oxygen detector combined with an InLab Optiox sensor. All experiments were performed at 30 °C and a constant concentration of fluorine (0.03 mmol/mL). For each measurement, pure oxygen was bubbled through the solutions until the dissolved oxygen concentration reached 33 mg/L (the saturation level of oxygen at 30 °C). The vials were then opened to allow oxygen to equilibrate with oxygen concentrations in air. The dissolved oxygen concentration was continuously monitored every 5 min for around 4 h. The oxygen concentrations were plotted with respect to time, and half-lives were obtained by fitting the curves to a first-order decay. Experiments were performed in triplicate, and the average results are shown in Figure 4 and Table 2.

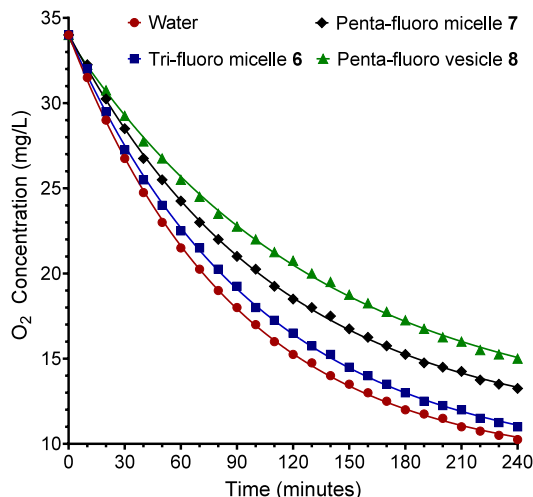


**Figure 4.** Oxygen solubility curves obtained at 30 °C for the polyfluoro and control systems. The fluorine concentration was constant at 0.03 mmol/mL for all fluorine systems. Data shown are the average from 3 experiments; plots for each system are included in the Supporting Information.

**Table 2. Oxygen Release and Half-Life Data for the Polyfluoro Diblock Self-Assembled Structures 2, 4, and 5<sup>a</sup>**

diblock polymer	fluorine concn (mmol/mL)	rate of O <sub>2</sub> release (×10 <sup>-3</sup> mg/L/min)	half-life (min)
control/water	0	11.1	63
trifluoro micelle 6	0.03	10.4	67
pentafluoro micelle 7	0.03	9.1	76
pentafluoro vesicle 8	0.03	7.3	95

<sup>a</sup>Data recorded at 30 °C. Fluorine concentrations calculated using the molecular weights from NMR. Data shown are the average from 3 experiments, with errors of 3, 14, 7, and 4% for the control, trifluoro micelle 6, pentafluoro micelle 7, and pentafluoro vesicle 8, respectively.

The oxygen level for the control/water system (no polymer) saturated with pure oxygen had a half-life of 63 min. The oxygen binding experiments were then repeated using the fluorinated systems 6–8. In all cases a longer half-life was recorded, confirming that all the fluorinated systems were able to bind oxygen and increase its concentration in water. However, despite the fluorine concentrations being identical for all polymer samples, the oxygen binding and release data were not the same. This suggests that oxygen binding was not simply a function of the fluorine concentration. When examining plots and decay data for the micellar systems in more detail, it was clear that the pentafluoro micelle 7 was able to bind around 10% more oxygen than the corresponding trifluoro micelle 6. This is likely due to the increased density of fluorine and higher relative concentration within the micellar core of the pentafluoro 7 system. As such, a superior electronic environment more conducive to oxygen binding is available within the core of pentafluoro micelle 7 (compared to trifluoro micelle 6). More interestingly, the data showed a clear relationship between the oxygen binding/release and the morphology of the self-assembled pentafluoro polymers. Specifically, the pentafluoro vesicle 8 had a half-life that was around 22% longer than the corresponding pentafluoro micelle 7 and 35% more than the trifluoro micelle 6. In addition, solutions of pentafluoro vesicle 8 could solubilize 53% more oxygen than water alone. Despite keeping the fluorine concentration constant in all experiments, the significantly longer half-life observed for pentafluoro vesicle 8 was unexpected. However, given the vesicle’s structure, it is probable that the increased binding is due to additional oxygen trapped within the inner aqueous portion of the vesicle. This extra oxygen can only be released once oxygen has been lost from both the aqueous phase and the fluorine component of the vesicle membrane. Figure 5 shows a schematic representation of the mechanism. Initially the release process is the same as that proposed for the micelles (Figure 3)<sup>18</sup> with oxygen in the aqueous phase reaching equilibrium with the oxygen levels in air. Next, oxygen bound within the membrane’s fluorine layer is released and diffuses into the aqueous layer before equilibrating with the oxygen levels in air. This leaves room within the fluorine layer that oxygen from the inner aqueous phase can fill, which then moves into the aqueous phase and eventually to air.

To test whether oxygen solubility was due to the fluorine content, additional controls were carried out. The first examined a solution containing just the mPEG component of the polymers, which produced an identical plot and kinetic data that were indistinguishable from the aqueous control. This confirmed that the mPEG component had no effect on the

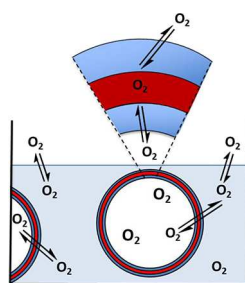


**Figure 5.** Schematic showing oxygen binding and release equilibria from the vesicle **8** solution saturated with 100% oxygen. The vesicle has an aqueous inner phase that can solubilize additional oxygen. The oxygen bound within can only leave after oxygen from the fluorinated membrane moves into the bulk aqueous phase, before it equilibrates with the levels of oxygen in air.

solubilization of oxygen, which is consistent with previous studies on the oxygen solubilization within PEG solutions.<sup>35</sup> An additional control, designed to test micellar solutions that did not contain fluorine, was also carried out. For this experiment we investigated an mPEG methacrylate diblock polymer **9** (mPEG-PMMA<sub>21</sub>) that was synthesized using the same mPEG macroinitiator and ATRP method described above in Scheme 1.<sup>18</sup> This non-fluorinated polymer formed micelles in aqueous solution and had very similar properties to the fluorinated systems **6** and **7**.<sup>36</sup> The oxygen binding and release experiment using this non-fluorinated micelle gave identical results to those obtained using mPEG or aqueous solutions.<sup>18,37</sup> Overall, these results provide solid evidence that oxygen solubility and binding were dependent on the fluorine content.

In a final experiment, the DLS measurements were repeated using oxygenated species. The results showed that the micellar systems increased in size by reproducible 3–4 nm in diameter. These results add even more support for oxygen binding within micellar systems. However, no discernible increase in size was observed when repeating the experiment using the pentafluoro vesicle **8**. However, this is not surprising when considering how much the fluorinated regions of the micelles and vesicles contribute to the overall size of each aggregated system. For example, the fluorinated regions of the micellar systems **6** and **7** make up a large part of their overall diameter. However, the fluorinated region of vesicle **8** is very small with respect to its overall size and does not contribute much to its diameter. Therefore, it is to be expected that any increase in the fluorinated region of vesicle **8** would not be accompanied by an observable increase in the overall size of the oxygenated vesicle.

#### 4. CONCLUSIONS

The results described herein are applicable to a number of areas where oxygen binding and sensing are important. However, the aim of this work was to increase aqueous oxygen concentrations, with a view toward developing new blood substitutes. Specifically, we aimed to synthesize and test self-assembled systems that were larger than the pore sizes in some vessel walls (100 nm). This is important because it reduces leakage from the vascular system and the toxic effects associated with the accumulation of oxygen within tissue. To achieve these goals, a series of fluorinated block copolymers that could self-assemble into micelles or vesicles were synthesized. The same mPEG macroinitiator was polymerized

with either 15 or 25 equiv of a pentafluoro monomer or 25 equiv of a trifluoro monomer under controlled ATRP conditions. Aggregation studies identified CAC values of 5.0  $\mu\text{g}/\text{mL}$  for both pentafluoro polymers **4** and **5** and 3.5  $\mu\text{g}/\text{mL}$  for the trifluoro polymer **2**. DLS analysis returned solvated sizes of around 30 nm for mPEG-PTF<sub>25</sub> **2** and mPEG-PPF<sub>15</sub> **4**, which are typical sizes for polymeric micelles.<sup>36</sup> The DLS data were supported by TEM, which showed clear images of spherical micelle structures for mPEG-PTF<sub>25</sub> **2** and mPEG-PPF<sub>15</sub> **4**. However, TEM could only identify partial and broken vesicle structures for the mPEG-PPF<sub>25</sub> **5** copolymer. This is a known phenomenon that can occur during the evaporation and preparation of samples for TEM analysis.<sup>28–30</sup> Nevertheless, DLS analysis of the mPEG-PPF<sub>25</sub> **5** copolymer indicated a solution diameter of around 350 nm, which is consistent with vesicle structures.<sup>27</sup>

Oxygen binding studies at 30 °C and a constant fluorine concentration of 0.03 mmol/mL indicated that all polymer solutions could dissolve more oxygen than water. When comparing the two micelle-based systems, it was clear that solutions of the pentafluoro micelle **7** could dissolve 10% more oxygen than the corresponding trifluoro micelle **6** and 23% more than water alone. This was due to the increased electronegative environment within the more fluorine dense core of pentafluoro micelle **7**. Of more note was the increased solubility of oxygen in solutions of the pentafluoro vesicle **8**, which could bind 22% and 35% more oxygen than the trifluoro micelle **6** and pentafluoro micelle **7**, respectively, and 53% more oxygen than water alone. In this case, the increase in oxygen solubility was due to the vesicle structure, which can accommodate additional oxygen within the aqueous interior. This additional oxygen is trapped within the interior and only liberated when oxygen bound within the fluorinated membrane is released back to bulk solvent and then air. The results described clearly demonstrate the importance of fluorine density and morphology in the ability of Nano objects to bind and release oxygen. Work is continuing within our laboratory to develop large systems that are more stable and can bind increased amounts of oxygen.

#### ■ ASSOCIATED CONTENT

##### SI Supporting Information

The Supporting Information is available free of charge at <https://pubs.acs.org/doi/10.1021/acsapm.4c00246>.

Characterization data and oxygen binding curves for all polymers (PDF)

#### ■ AUTHOR INFORMATION

##### Corresponding Author

Lance J. Twyman — Department of Chemistry, University of Sheffield, Sheffield, South Yorkshire, U.K. S3 7HF;  
 orcid.org/0000-0002-6396-8225; Email: l.j.twyman@sheffield.ac.uk

##### Author

Zerui Chen — Department of Chemistry, University of Sheffield, Sheffield, South Yorkshire, U.K. S3 7HF

Complete contact information is available at: <https://pubs.acs.org/doi/10.1021/acsapm.4c00246>

##### Notes

The authors declare no competing financial interest.

## REFERENCES

- (1) Di Monte, R.; Kašpar, J. On the Role of Oxygen Storage in Three-Way Catalysis. *Top. Catal.* **2004**, *28*, 47–57.
- (2) Ciriminna, R.; Campestri, S.; Pagliaro, M. Fluorinated Silica Gels Doped with TPAP as Effective Aerobic Oxidation Catalysts in Dense Phase Carbon Dioxide. *Adv. Synth. Catal.* **2004**, *346*, 231–236.
- (3) Que, Y.; Ruan, J.; Xiao, Y.; Feng, C.; Lu, G.; Huang, X. Fluorinated vesicles embedded with Ru-based catalysts as efficient and recyclable nanoreactors for photo-mediated aerobic oxidation. *Polym. Chem.* **2020**, *11*, 1727–1734.
- (4) Mills, A.; Lawrie, K.; Bardin, J.; Apedaile, A.; Skinner, G. A.; O'Rourke, C. An O<sub>2</sub> smart plastic film for packaging. *Analyst* **2012**, *137*, 106–112.
- (5) Gillanders, R. N.; Tedford, M. C.; Crilly, P. J.; Bailey, R. T. Thin film dissolved oxygen sensor based on platinum octaethylporphyrin encapsulated in an elastic fluorinated polymer. *Anal. Chim. Acta* **2004**, *502*, 1–6.
- (6) Jiang, X.; Chun, F.; Lu, G.; Xiaoyu, H. Oxygen and carbon dioxide dual gas-responsive homopolymers and diblock copolymers synthesized via RAFT polymerization. *Polym. Chem.* **2017**, *8*, 1163–1176.
- (7) Vigiak, O.; Grizzetti, B.; Udias-Moinelo, A.; Zanni, M.; Dorati, C.; Bouraoui, F.; Pistocchi, A. Predicting biochemical oxygen demand in European freshwater bodies. *Science of The Total Environment*. **2019**, *666*, 1089–1105.
- (8) Ahmed, A. K. A.; Shi, X.; Hua, L.; Manzueta, L.; Qing, W.; Marhaba, T.; Zhang, W. Influences of Air, Oxygen, Nitrogen, and Carbon Dioxide Nanobubbles on Seed Germination and Plant Growth. *J. Agric. Food Chem.* **2018**, *66* (20), 5117–5124.
- (9) Workie, Y. A.; Kuo, C. Y.; Riskawati, J. H.; Krathumkhet, N.; Imae, T.; Ujihara, M.; Krafft, M. P. Hierarchical Composite Nanoarchitectonics with a Graphitic Core, dendrimer and fluorocarbon domains, and a poly(ethylene glycol) shell as O<sub>2</sub> reservoirs for reactive oxygen species production. *ACS Appl. Mater. Interfaces* **2022**, *14* (30), 35027–35039.
- (10) Taylor, N. G.; Chung, S. H.; Kwansa, A. L.; Johnson, R. R.; Teator, A. J.; Milliken, N. B.; Koshlap, K. M.; Yingling, Y. G.; Lee, Y. Z.; Leibfarth, F. A. Partially Fluorinated Copolymers as Oxygen Sensitive 19 F MRI Agents. *Chemistry a European Journal* **2020**, *26* (44), 9982–9990.
- (11) Lui, F. E.; Kluger, R. Reviving artificial blood: meeting the challenge of dealing with no scavenging by hemoglobin. *Chem. Bio. Chem.* **2010**, *11* (13), 1816–1824.
- (12) Riess, J. G. Oxygen carriers (“blood substitutes”) raison d’être, chemistry, and some physiology. *Chem. Rev.* **2001**, *101* (9), 2797–2920.
- (13) Twyman, L. J.; Ge, Y. Porphyrin cored hyperbranched polymers as heme protein model. *Chem. Commun.* **2006**, No. 15, 1658–1660.
- (14) Ferenz, K. B.; Steinbicker, A. U. Artificial Oxygen Carriers - Past, Present and the Future-a Review of the Most Innovative and Clinically Relevant Concepts. *J. Pharmacol. Exp. Ther.* **2019**, No. jpet.118.254664.
- (15) Riess, J. G. Overview of Progress in the Fluorocarbon Approach to in vivo Oxygen Delivery. *Biomater. Artif. Cell Im.* **1992**, *20* (2–4), 183–202.
- (16) Flaim, S. F. Pharmacokinetics and Side Effects of Perfluorocarbon-Based Blood Substitutes. *Artif. Cells, Blood Substitutes, Biotechnol.* **1994**, *22* (4), 1043–1054.
- (17) Porter, C. J. H.; Moghimi, S. M.; Illum, L.; Davis, S. S. The Polyoxyethylene/Polyoxypropylene Block Co-Polymer Poloxamer-407 Selectively Redirects Intravenously Injected Microspheres to Sinusoidal Endothelial Cells of Rabbit Bone Marrow. *FEBS Lett.* **1992**, *305* (1), 62–66.
- (18) Fan, M.; Alghassab, T. S.; Twyman, L. J. Increased Oxygen Solubility in Aqueous Media Using PEG-Poly- 2,2,2-Trifluoroethyl Methacrylate Copolymer Micelles and Their Potential Application as Volume Expanders and as an Artificial Blood Product. *ACS Appl. Bio Mater.* **2018**, *1* (3), 708–713.
- (19) Xiong, Y.; Liu, Z. Z.; Georgieva, R.; Smuda, K.; Steffen, A.; Sendeski, M.; Voigt, A.; Patzak, A.; Bäuml, H. Nonvasoconstrictive Hemoglobin Particles as Oxygen Carriers. *ACS Nano* **2013**, *7* (9), 7454–7461.
- (20) Liu, H.; Zhang, S.; Huang, X.; Ding, A.; Lu, G. Construction of well-defined difluoromethylthio-containing amphiphilic homopolymers by RAFT polymerization. *Polym. Chem.* **2020**, *11*, 7542–7550.
- (21) Aguiar, J.; Carpena, P.; Molina-Bolívar, J. A.; Carnero Ruiz, C. On the Determination of the Critical Micelle Concentration by the Pyrene 1:3 Ratio Method. *J. Colloid Interface Sci.* **2003**, *258* (1), 116–122.
- (22) Blanz, A.; Armes, S. P.; Ryan, A. J. Self-Assembled Block Copolymer Aggregates: From Micelles to Vesicles and their Biological Applications. *Macromol. Rapid Commun.* **2009**, *30*, 267–277.
- (23) Wang, J. S.; Matyjaszewski, K. Controlled “Living” Radical Polymerization. Halogen Atom Transfer Radical Polymerization Promoted by a Cu(I)/Cu(II) Redox Process. *Macromolecules* **1995**, *28* (23), 7901–7910.
- (24) Semsarilar, M.; Jones, E. R.; Armes, S. P. Comparison of Pseudo-Living Character of RAFT Polymerizations Conducted under Homogeneous and Heterogeneous Conditions. *Polym. Chem.* **2014**, *5* (1), 195–203.
- (25) Pang, B.; Liu, R.; Han, G.; Wang, W.; Zhang, W. The Synthesis of Thermoresponsive POSS-Based Eight-Arm Star Poly(: N -Isopropylacrylamide): A Comparison between Z-RAFT and R-RAFT Strategies. *Polym. Chem.* **2021**, *12* (14), 2063–2074.
- (26) Ananthapadmanabhan, K. P.; Goddard, E. D.; Turro, N. J.; Kuo, P. L. Fluorescence Probes for Critical Micelle Concentration. *Langmuir* **1985**, *1* (3), 352–355.
- (27) Zhu, Y.; Yang, B.; Chen, S.; Du, J. Polymer Vesicles: Mechanism, Preparation, Application, and Responsive Behavior. *Prog. Polym. Sci.* **2017**, *64*, 1–22.
- (28) Gaitzsch, J.; Messenger, L.; Morecroft, E.; Meier, W. Vesicles in Multiple Shapes: Fine-Tuning Polymersomes’ Shape and Stability by Setting Membrane Hydrophobicity. *Polymers* **2017**, *9*, 483.
- (29) Cizmar, P.; Yuana, Y. Detection and Characterization of Extracellular Vesicles by Transmission and Cryo-Transmission Electron Microscopy. *Methods Mol. Biol.* **2017**, *1660*, 221–232.
- (30) Yang, J.; Piñol, R.; Gubellini, F.; Lévy, D.; Albouy, P. A.; Keller, P.; Li, M. H. Formation of Polymer Vesicles by Liquid Crystal Amphiphilic Block Copolymers. *Langmuir* **2006**, *22* (18), 7907–7911.
- (31) Huang, C.; Quinn, D.; Sadovskiy, Y.; Suresh, S.; Hsia, K. J. Formation and size distribution of self-assembled vesicles. *Proc. Natl. Acad. Sci. U. S. A.* **2017**, *114* (11), 2910–2915.
- (32) Palumbo, F. S.; Di Stefano, M.; Palumbo Piccionello, A.; Fiorica, C.; Pitarresi, G.; Pibiri, I.; Buscemi, S.; Giammona, G. Perfluorocarbon Functionalized Hyaluronic Acid Derivatives as Oxygenating Systems for Cell Culture. *RSC Adv.* **2014**, *4* (44), 22894–22901.
- (33) Demas, J. N.; DeGraff, B. A.; Coleman, P. B. Peer Reviewed: Oxygen Sensors Based on Luminescence Quenching. *Anal. Chem.* **1999**, *71* (23), 793A–800A.
- (34) Pitarresi, G.; Piccionello, A. P.; Calabrese, R.; Pace, A.; Buscemi, S.; Giammona, G. Fluorinated Derivatives of a Polyaspartamide Bearing Polyethylene Glycol Chains as Oxygen Carriers. *J. Fluor. Chem.* **2008**, *129* (11), 1096–1103.
- (35) Mexal, J.; Fisher, J. T.; Osteryoung, J.; Reid, C. P. P. Oxygen Availability in Polyethylene Glycol Solutions and Its Implications in Plant-Water Relations. *Plant. Physiol.* **1975**, *55*, 20–24.
- (36) The mPEG-PMMA21 diblock polymer 9 had a molecular weight of 4200 (by NMR) and a degree of polymerization of 21. It had an average diameter of 40 nm as determined by DLS and TEM and a CAC of 3.6 mg/mL (see refs 17 and 35).
- (37) Meng, F. The Synthesis and Oxygen Binding Properties of Self-assemble Fluorinated Copolymers and Their Possible Application as Blood Substitutes. Ph.D. Dissertation, University of Sheffield: UK, 2020. <https://etheses.whiterose.ac.uk/27527/> (accessed 2024-01-23).